Macromolecules

ARTICLE

pubs.acs.org/Macromolecules

# Rheology and Phase Behavior of Lyotropic Cellulose Nanocrystal Suspensions

Esteban E. Ureña-Benavides,[†] Geyou Ao,[‡] Virginia A. Davis,[‡] and Christopher L. Kitchens*[,†]

[†]Department of Chemical and Biomolecular Engineering, Clemson University, Clemson, South Carolina 29634, United States

[‡]Department of Chemical Engineering, Auburn University, Auburn, Alabama 36849, United States

Supporting Information

**ABSTRACT:** The dispersion microstructure and rheological properties of aqueous sulfonated cellulose nanocrystal (CNC) suspensions have been investigated. Between 3.07 and 10.4 vol % the suspensions phase separated into liquid crystalline and isotropic domains. At 12.1 vol %, no isotropic phase was visible, and the samples had the fingerprint texture characteristic of a cholesteric liquid crystal. Below 35 °C, temperature had little influence on rheology and phase behavior. However, between 35 and 40 °C there was a significant change in both the fraction of isotropic phase and the rheological properties. In contrast to many lyotropic suspensions, the steady shear viscosity did not go through a maximum with increasing concentration. Maxima were observed for complex viscosity, storage modulus, and loss modulus at concentrations that appeared fully liquid crystalline. Time−concentration superposition was successful for the loss modulus but not the storage modulus. This suggests that the interface in biphasic samples affects the elastic relaxation but not the viscous response. At still higher concentrations, the fingerprint texture of the liquid crystal phase was absent, and the dispersions behaved as rheological gels.

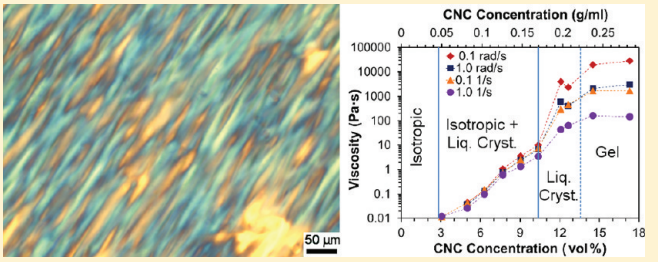


## INTRODUCTION

Cellulose nanocrystals (CNC) are renewable, strong, lightweight, and low-cost nanomaterials that have been incorporated into renewable polymer matrices for sustainable, environmentally friendly nanocomposites[1,2] and assembled into optically active films that selectively reflect specific wavelengths of light.[3,4] CNC are commonly isolated from native cellulosic materials by acid hydrolysis where the CNC size and surface chemistry depend on the cellulose source and reaction conditions. Aqueous suspensions of sulfonated CNC exhibit lyotropic phase behavior, readily transitioning from isotropic to a biphasic suspension to a liquid crystalline phase with increasing concentration.[5,6] At still higher concentrations, the suspensions can transition into a birefringent gel-like material.[7]

The properties of bulk CNC-based materials produced by fluid phase processing are dependent on the type of CNC employed, the dispersion microstructure, and the processing conditions.[8,9] CNC tend to assemble in cholesteric liquid crystals;[6] moreover, blending CNC with macromolecules such as alginate[10] or inorganic materials like silica[3] can induce similar types of ordering in the resultant mixtures. The optical properties of films assembled from CNC dispersions can be tuned by controlling the cholesteric pitch which can be affected by dispersion composition, temperature, and shear.[11] The mechanical properties of CNC−calcium alginate fibers have been shown to be dependent on the helical assembly of the cellulose crystallites, which is observed in nature and interrelated with the cholesteric ordering of CNC suspensions.[10,12] Therefore, understanding the rheology and phase behavior of CNC dispersions is of both scientific interest and practical relevance.

At the critical concentration for the isotropic to biphasic transition, the larger particles first form the liquid crystalline phase, while the smallest remain in the isotropic phase.[13,14] Thus, the size distribution is an important parameter affecting the phase behavior.[5,13] The ionic strength of the medium also has an important effect.[15] Sulfonated CNC are intrinsically acidic; consequently, any variation of concentration induces a change of the ionic strength, yielding a nonlinear behavior of the phase transition diagram and equilibrium concentrations.[15] It has been shown that increasing temperature also impacts the phase behavior by decreasing the volume of the liquid crystalline phase, especially near 40 °C.[16] Still, limited information exists regarding the interrelations of phase behavior with rheological properties and the transition into a hydrogel material at high CNC concentrations.

A small-angle scattering study by Orts et al. confirmed that a concentrated CNC suspension isolated from black spruce bleached Kraft pulp was chiral nematic (cholesteric) at rest, yet the particles oriented with the larger axis parallel to the direction of the flow as the shear rate was increased.[17] Suspensions of micrometer length CNC derived from tunicate showed a very

**Received:** July 18, 2011
**Revised:** September 9, 2011
**Published:** October 24, 2011

small reduction of viscosity upon appearance of a liquid crystalline phase followed by a monotonic increase in viscosity with concentration.[18] A three-region behavior was observed for the liquid crystalline samples, while the isotropic suspensions behaved as classic polymer solutions.[18]

In this study, we report the effects of concentration and temperature on the microstructure and shear response of aqueous sulfonated cellulose nanocrystal dispersions. In contrast to most previous studies,[17,18] we evaluated the phase behavior using a combination of both low-magnification imaging and hot stage cross-polarized optical microscopy. We also evaluated the viscoelastic properties in addition to the steady shear response. This more detailed understanding of the rheology and phase behavior of cellulose nanocrystal dispersions will aid in developing CNC composite materials with controlled properties.

## EXPERIMENTAL SECTION

**Isolation of Cellulose Nanocrystals (CNC).** Whatman (Piscataway, NJ) cellulose filter aid (cotton powder) was used as the raw material for CNC isolation. The CNC were isolated via acid hydrolysis of cotton cellulose with 64 wt % sulfuric acid at 45 °C for 50 min. Upon completion, the reaction was quenched with cold deionized water. The resulting slurry was allowed to precipitate, and the supernatant was decanted. The solids were dialyzed against deionized water for several days until the pH remained constant. Ultrasonication was used to redisperse the CNC in water. The batch was divided into several samples, and the concentration of each was adjusted by slowly evaporating the water under a nitrogen stream. The concentration was measured in wt % and transformed to g/mL and vol % using the densities of water and CNC at 25 °C, which are 0.9970 and 1.636 g/mL, respectively. Further details of CNC isolation can be found elsewhere.[10,13]

**Size Characterization.** A Digital Instruments/Veeco Bioscope atomic force microscope (Plainview, NY) was used in tapping mode to measure the dimensions of the CNC. A droplet of a CNC suspension with an approximate concentration of 0.01 wt % was allowed to dry on a freshly cleaved mica surface (~1.5 $cm^2$).[19] In order to avoid artifacts due to particles lying on top of another, only the 117 CNC that seemed isolated were included in the statistics. The tip employed had a nominal radius of less than 10 nm. An image of the tip was obtained using a porous aluminum standard surface; this image was used to deconvolute the shape of the particles from the geometry of the tip.[20] Both the standard surface and the tip were purchased from MikroMasch (San Jose, CA).

**Imaging of Bulk Samples.** Samples of 2.99, 3.85, 4.83, and 6.23 vol % were introduced into 2 mm path length sealed quartz cuvettes and allowed to rest for at least 12 days at the desired temperature. The cuvettes were placed between crossed polarized films, and pictures were taken using a digital camera. The percent liquid crystalline phase was measured from the images.[14,15] The experiments were performed at 4, 20, and 45 °C; the same cuvettes were used at all temperatures. Before each measurement, the samples were homogenized using a vortex stirrer.

**Polarized Light Microscopy.** A droplet of each suspension was placed on a temperature-controlled stage or microscope slide. Pictures were taken with a Nikon (Melville, NY) Eclipse 80i optical microscope using an LU Plan Fluor 20*x*/0.45NA Nikon objective lens at room temperature. For higher temperature imaging, a Linkam (Tadworth, UK) optical rheology system CSS450 was used with an L Plan SLWD 20*x*/0.35NA Nikon objective lens.

**Rheological Measurements.** Aqueous suspensions with CNC concentrations ranging from 3.07 to 17.3 vol % were analyzed using an Anton Paar (Ashland, VA) MCR301 rotational rheometer. Steady shear viscosity versus shear rate curves were generated for each sample from a shear rate of 0.1 to 100 $s^{-1}$. For each sample, the time required to reach steady state at 0.1 $s^{-1}$ was determined by a transient test; the sampling time used to generate the flow curves was decreased linearly with increasing shear rate. Oscillatory measurements were also performed on each sample from 0.1 to 100 rad/s. The percent strain used was inside the linear viscoelastic region (LVE) as determined by performing amplitude sweep experiments at a frequency of 10 rad/s. All the suspensions were tested at 10 °C; the effect of temperature on the steady shear viscosities was also studied for samples of 3.07, 6.99, and 12.1 vol %. The low-viscosity samples were characterized using Mooney-Ewart or double gap geometries; the high-viscosity samples were measured using 25 mm parallel plates and cone and plate (2° nominal angle) geometries. For several samples, two different geometries were used to ensure no experimental artifacts were present. All data are presented with error bars generated from the standard deviation.

## RESULTS AND DISCUSSION

**CNC Properties.** Since phase behavior is influenced by both mesogen size and electrostatic stabilization, the size distribution and the proportion of sulfate groups were measured. The size distributions of the CNC measured with atomic force microscopy (AFM) are shown in Figure 1; they were elongated particles with rectangular cross section.[10,21,22] The average length was 107 nm with a standard deviation ($\sigma$) of 55 nm, the average width was 20 nm ($\sigma$ = 6 nm), and the average height was 8.9 nm ($\sigma$ = 2.8 nm). The polydispersity defined as $p = [(\langle a^2\rangle - \langle a\rangle^2)/\langle a\rangle^2)]^{1/2}$ was also calculated. Here $\langle a^2\rangle$ and $\langle a\rangle$ are the second and first moments of $a$, respectively, while $a$ is any dimension. For length, width, and height $p$ is 0.52, 0.29, and 0.32, respectively. The CNC suspensions were acidic due to the presence of $-SO_3H$ groups introduced on the surface of the nanocrystals during the hydrolysis step. A suspension of 1.59 vol % had a pH of 2.9. Conductometric titration with sodium hydroxide ($4.2 \times 10^{-3}$ M) was used to determine that there were $1.71 \times 10^{-4}$ mol of $-SO_3H$ per gram of cellulose, which, according to our size measurements, is equivalent to sulfonating 30% of the available primary hydroxyl groups.

**Phase Behavior and Microstructure.** Revol et al. first observed that biphasic suspensions of sulfonated CNC consist of isotropic and chiral nematic (cholesteric) phases that readily phase separate and can be observed by simply placing cuvettes between cross-polarized films.[6] Figure 2 shows four suspensions imaged between crossed polarizers; the fraction of the bottom birefringent liquid crystalline phase increased with increasing CNC concentration. The amount of liquid crystalline phase as a function of CNC concentration was determined at three different temperatures (Figure 3). No significant difference was observed between 4 and 20 °C, but at 45 °C the volume of liquid crystalline phase at a given concentration was reduced; this is analogous to the behavior previously observed by Dong and Gray.[16] Moreover, the slope of the trendline decreases at higher temperatures, suggesting an enlargement of the biphasic region.

The isotropic to biphasic transition concentrations $\phi_I$ were measured by extrapolation of the curves in Figure 3; the results were 2.8, 2.7, and 3.0 vol % at 4, 20, and 45 °C, respectively. Our measurement at 20 °C is in very good agreement with the transition concentration reported by Dong and Gray of $5.14 \times 10^{-6}$ $nm^{-3}$ (2.9 vol % for their average dimensions and assuming a squared rod geometry).[16] However, it was not possible to accurately quantify the biphasic to liquid crystalline transition

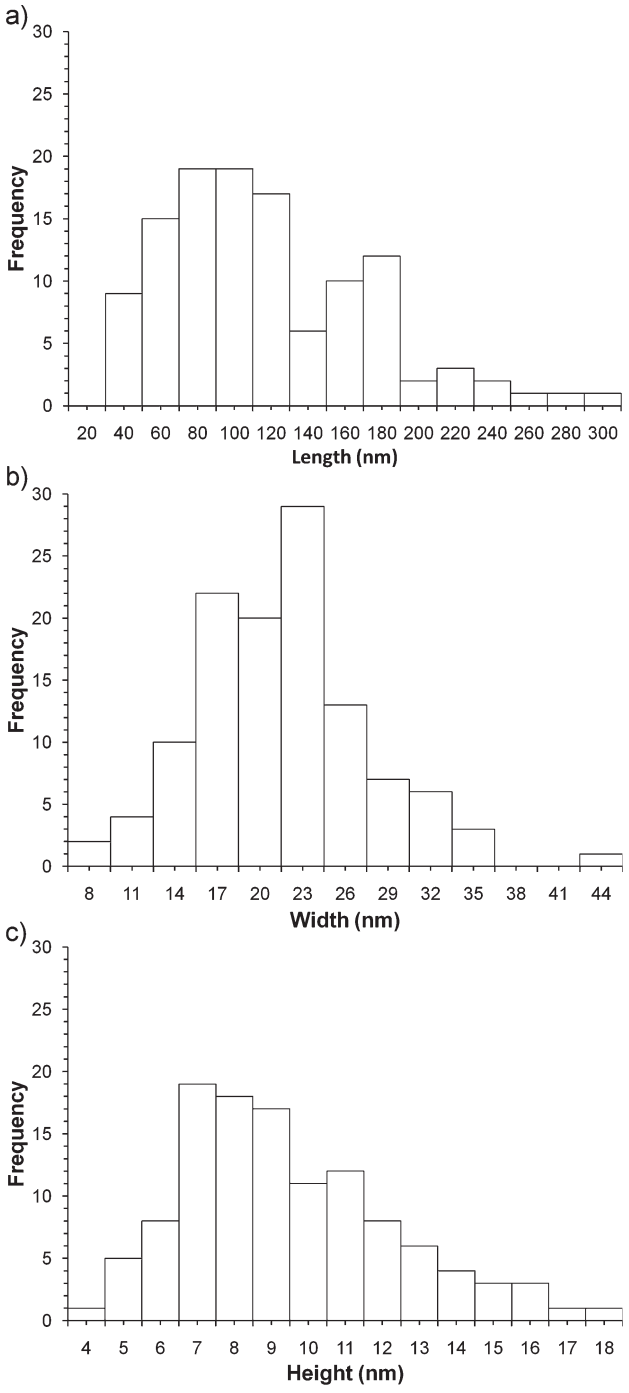


**Figure 1.** Size distribution of CNC (a) length, (b) width, and (c) height.

concentration $\phi_{LC}$ using the same method. At CNC concentrations from 7.69 to 10.4 vol % the sample looked completely birefringent in the cuvettes, but optical microscopy revealed isotropic regions. The viscosity of these biphasic suspensions likely prevented complete separation of the liquid crystalline and isotropic phases within the 12 days of settling time; the size of the isotropic domains was too small to be observed without magnification. Centrifugation of the suspensions was attempted to accelerate phase separation of the higher concentration biphasic samples. Measurements of the relative volume of the anisotropic

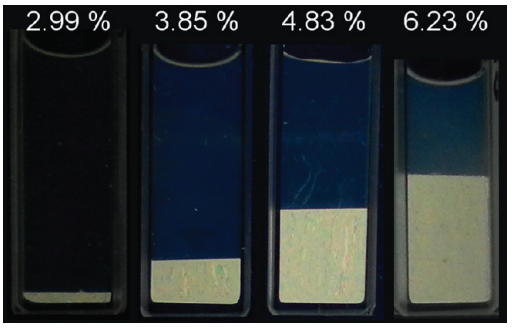


**Figure 2.** Cross-polarized images showing the phase separation of CNC suspensions from 2.99 to 6.23 vol %. The lower liquid crystalline phase is birefringent while the upper isotropic phase appears dark.

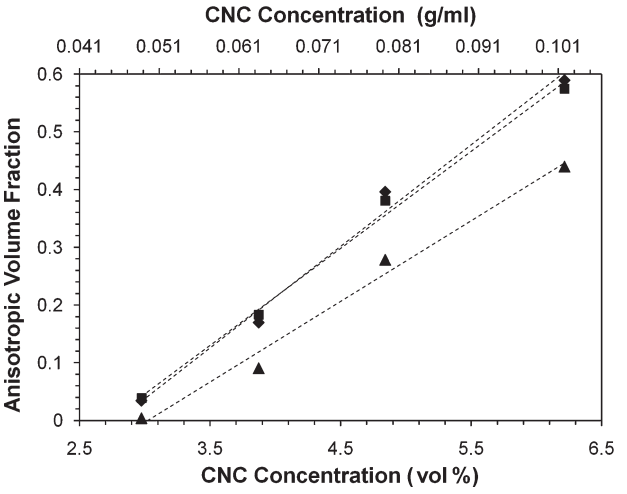


**Figure 3.** Amount of liquid crystalline (anisotropic) phase as a function of CNC concentration at 4 °C (diamonds), 20 °C (squares), and 45 °C (triangles).

phase and extrapolation to one (completely anisotropic) yielded a $\phi_{LC}$ of 11.2 vol %. The technique proves to be useful to aid separation, yet care must be taken to avoid heating the sample and/or precipitating nanoparticles out of the suspension.

Representative cross-polarized optical microscopy images of increasing CNC concentration are shown in Figure 4 (additional representative images from several concentrations taken at different angles are provided in the Supporting Information). At 5.00 vol % it was possible to observe the presence of liquid crystalline droplets dispersed in a continuous isotropic phase. Rotation of the sample between cross polarizers caused the bright regions (liquid crystalline) to darken while the continuous isotropic domain remained unchanged. As the concentration was increased to 6.30 vol %, the fraction of liquid crystal domains increased, and the microstructure was suggestive of a cocontinuous mixture of isotropic and liquid crystalline regions. However, after 12 days settling in a cuvette, demixing occurred and the volume fraction of the anisotropic region was ~0.6 between 4 and 20 °C (Figure 3). At 9.03 vol %, the suspension looked completely birefringent in a cuvette; however, under the microscope isotropic regions were observed in a liquid crystalline matrix.

The sample containing 9.91 vol % CNC appeared almost entirely liquid crystalline under cross-polarized optical microscopy with 20× magnification; a few isotropic sections could be

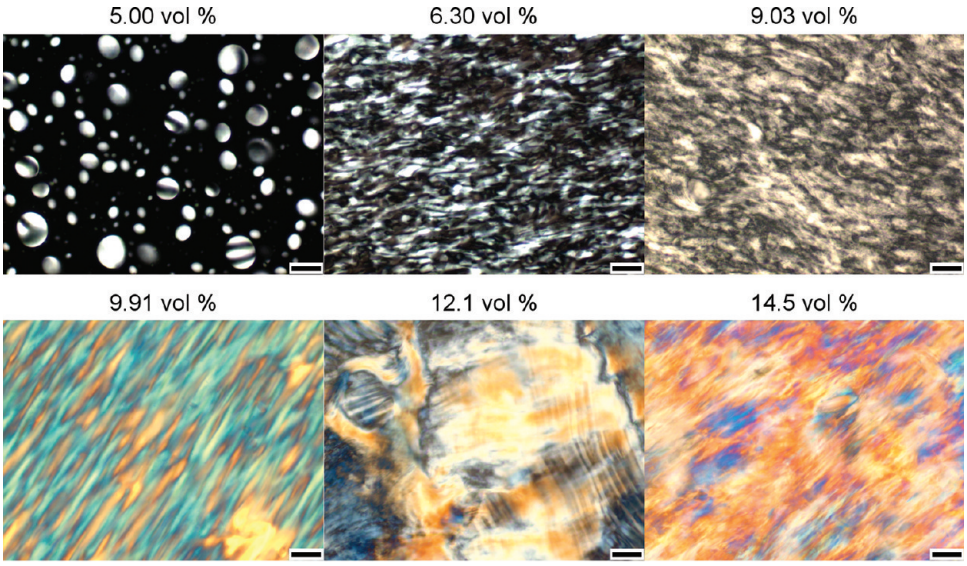


**Figure 4.** Polarized light microscopy of CNC suspensions of various concentrations at 25 °C. Scale bars: 50 $\mu$m.

observed near the sample edges. The colorful discontinuous stripes indicate a precholesteric type of ordering. Some isotropic regions were also observed at 10.4 vol %. However, at 12.1 vol %, the suspension was completely birefringent with colors that changed with rotation at all positions including the edge. Moreover, the stripes became uniform and formed the fingerprint texture which is characteristic of a cholesteric liquid crystal.

Based on these cross-polarized optical microscopy results 10.4 vol % < $\phi_{LC}$ < 12.1 vol %. While the cuvettes could not be used to quantify $\phi_{LC}$, the value of 11.2 vol % measured by centrifugation is consistent with the microscopy results. Dong and Gray measured a lower critical concentration of $15.3 \times 10^{-6}$ nm$^{-3}$ ($\phi_{LC}$ = 8.6 vol %).[16] Nevertheless, they used the cuvettes for this purpose, which may explain the differences in the reported value. The discrepancies found with the various techniques highlight the need for developing standard methods for determining $\phi_{LC}$ for lyotropic nanorod dispersions.[23]

Theoretical calculations based on the Stroobants, Lekkerkerker and Odijk (SLO) theory were performed to compare with the experimental critical concentrations.[15,24,25] To account for variations in the ionic strength of the medium, the acid dissociation constant p$K_a$ of the sulfate groups was determined by conductometric titration. This yielded a value of 3.20, which was used to calculate the pH of the medium with variable CNC concentration. The calculated values for $\phi_I$ and $\phi_{LC}$ are 8.9 and 12.4 vol %, respectively. The theoretical prediction for $\phi_{LC}$ is very close to our experimental measurements; nevertheless, $\phi_I$ is clearly overestimated. It must be noted that the SLO theory was developed for rod-shaped particles while CNCs resemble more rectangular parallelepipeds. Moreover, the calculations assumed a monodispersed population with dimensions equal to the averages measured by AFM. Polydispersed samples are expected to show a broader biphasic region and shift $\phi_I$ to lower concentrations due to the presence of larger particles. Both phenomena are reflected in our experimental measurements.

When the CNC concentration reached 14.5 vol %, the texture (Figure 4) was more random with very bright colors; rheological characterization at this concentration revealed that the system was a gel. A similar behavior was observed in aqueous mixtures of single-walled carbon nanotubes (SWNTs) and double-stranded DNA; these suspensions formed a cholesteric phase which disappeared at high concentrations.[26]

**Effect of Temperature on Viscosity.** For many nanocylinder dispersions, including carbon nanotubes in superacids, both the phase boundaries and steady shear viscosities have shown little or no temperature dependence.[23] In the case of the CNC dispersions, some variations in microstructure were observed particularly between 20 and 45 °C (Figure 3). Since rheological behavior is directly affected by dispersion microstructure, the effect of temperature on the steady shear viscosity was measured for the predominantly isotropic 3.07 vol % sample, the predominantly liquid crystalline 6.99 vol % sample, and the liquid crystalline 12.1 vol % sample; the data are shown in Figure 5. The 3.07 vol % had a large Newtonian plateau at all measured temperatures; the inception of a shear thinning region at 30 s$^{-1}$ was apparent at 10 and 25 °C. As expected for a predominantly isotropic dispersion, the viscosity decreased with increasing temperature.

For the biphasic 6.99 vol % sample (Figure 5b), the three-region behavior typically associated with lyotropic polymer liquid crystals was observed.[27] The origin of region I, the initial shear thinning region, remains controversial[28,29] but is generally associated with variations on the disclination lines of the polydomain texture.[30] Director wagging[31] and alignment in the vorticity direction[32] have been reported at the intermediate region II. Region III, which has a lower slope than region I, is associated with particles alignment in the flow direction. This behavior has also been observed for attractive emulsions[32] and lyotropic SWNT dispersions in superacids.[33] For the CNC dispersions, three-region behavior was apparent at all three temperatures tested, but while the viscosity generally decreased with increasing temperature, little effect was observed in region I. Interestingly, region II was much more pronounced than for lyotropic SWNT−superacid dispersions.[33] Longer rods have larger rotational relaxation times and thus shear thin at lower shear rates.[34] Since SWNTs are longer and more polydisperse than CNCs, the range of shear rates at which region II is discernible may be reduced. Data for 40 °C are not shown because the microstructure

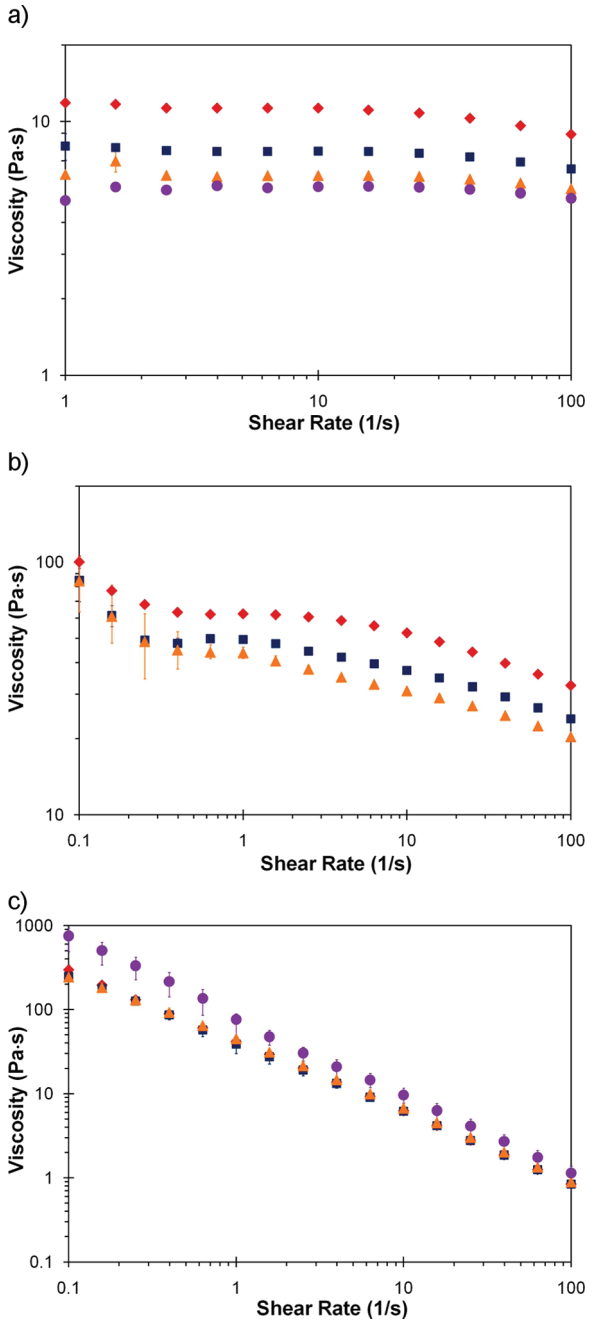


**Figure 5.** Steady shear viscosity versus shear rate at 10 (red diamonds), 25 (blue squares), 35 (orange triangles), and 40 °C (purple circles) of CNC suspensions with concentrations of (a) 3.07, (b) 6.99, and (c) 12.1 vol %.

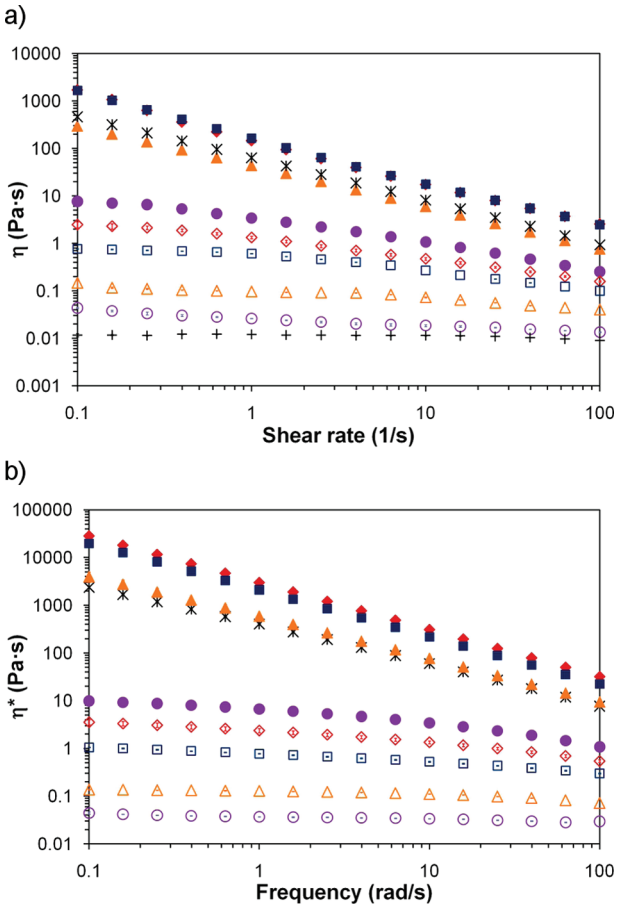


**Figure 6.** (a) Steady shear and (b) complex viscosities of CNC suspensions at 17.3 vol % (red solid diamonds), 14.5 vol % (blue solid squares), 12.6 vol % (black stars), 12.1 vol % (orange solid triangles), 10.4 vol % (purple solid circles), 9.03 vol % (red open diamonds), 7.69 vol % (blue open squares), 6.30 vol % (orange open triangles), 5.00 vol % (purple open circles), and 3.07 vol % (black crosses).

was not stable at these conditions; this caused large variations in the rheological measurements which are not unexpected for samples near the center of the biphasic region.

For the 12.1 vol % sample the viscosity was independent of temperature between 10 and 35 °C. This result suggests that in spite of the relatively low aspect ratio of the CNC, temperature had little effect on mesogen rearrangement between 10 and 35 °C. Interestingly, there was a marked viscosity increase at 40 °C, particularly at low shear rates. Despite the use of an evaporation blocker, the possibility that the suspension suffered from water evaporation was considered. However, this would have likely led to a greater deviation at longer measurement times which corresponded to higher shear rates. For lyotropic systems, temperature changes in viscosity can also be indicative of changes in microstructure or the relative fractions of isotropic and liquid crystalline regions.[35] Hot stage optical microscopy revealed a pronounced increase in isotropic domains between 35 and 40 °C (shown in Figure S5 of the Supporting Information); this confirmed that the observed change in viscosity was not an artifact.

**Effect of Concentration on Steady Shear and Complex Viscosities.** The dependence of the steady shear $\eta$ and complex $\eta^*$ viscosities for each suspension at 10 °C is shown in Figure 6. As previously described, at the lowest concentration, the behavior was nearly Newtonian with the inception of a shear thinning region at 30 $s^{-1}$; even at 3.07 vol % the viscosity was an order of magnitude greater than that of the solvent. The 5.00 and 6.30 vol % suspensions had a three-region behavior like that observed in Figure 5b for the 6.99 vol % sample, but this is masked by the scale of Figure 6a. Between 7.69 and 10.4 vol %, a low shear/frequency plateau is followed by a shear thinning region. At 12.1 vol % and above, the samples are power law fluids $\eta = K\dot{\gamma}^{n-1}$ where $\dot{\gamma}$ is the shear rate, $K$ is the consistency coefficient, and $n$ is the rate index. The power law coefficients for each sample are

**Table 1. Consistency and Rate Index of CNC Suspensions Behaving as Power Law Fluids**

| | complex viscosity | | steady shear viscosity | |
|---|---|---|---|---|
| CNC conc (vol %) | *K* | *n* | *K* | *n* |
| 12.1 | 573 | 0.122 | 42 | 0.138 |
| 12.6 | 386 | 0.172 | 62 | 0.103 |
| 14.5 | 2085 | 0.019 | 168 | 0.055 |
| 17.3 | 2965 | 0.017 | 161 | 0.065 |

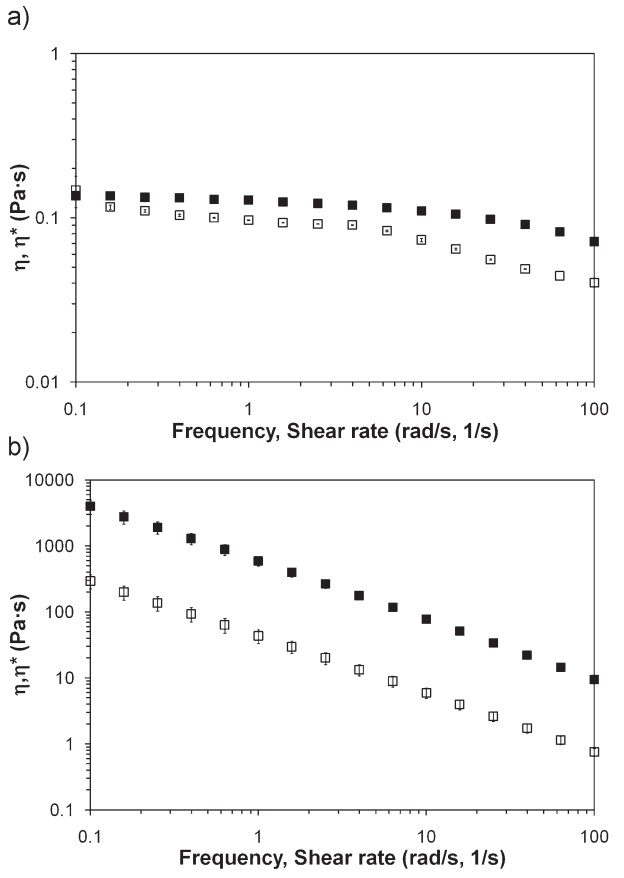


**Figure 7.** Cox−Merz rule comparison of samples containing (a) 6.30 and (b) 12.1 vol %. The open symbols represent the steady shear viscosity, and the solid symbols denote complex viscosity.

shown in Table 1; the marked transition in coefficient and power law index between 12.6 and 14.5 vol % occurred at the liquid crystalline to gel transition.

A common characteristic of lyotropic macromolecular liquid crystals is that the Cox−Merz rule is not obeyed; i.e., the steady and dynamic viscosities are not equal when the shear rate $\dot{\gamma}$ equals the frequency $\omega$. Figure 7 compares the steady and complex viscosities at 6.30 and 12.1 vol %. The lower concentration sample, where the system is more isotropic, showed little deviation from the Cox−Merz rule at low shear rate/frequency but greater deviation at high shear rate/frequency. The predominantly liquid crystalline samples and the birefringent gels deviated significantly from the Cox−Merz rule throughout the entire shear rate/frequency range, which is expected for suspensions containing oriented domains.[33]

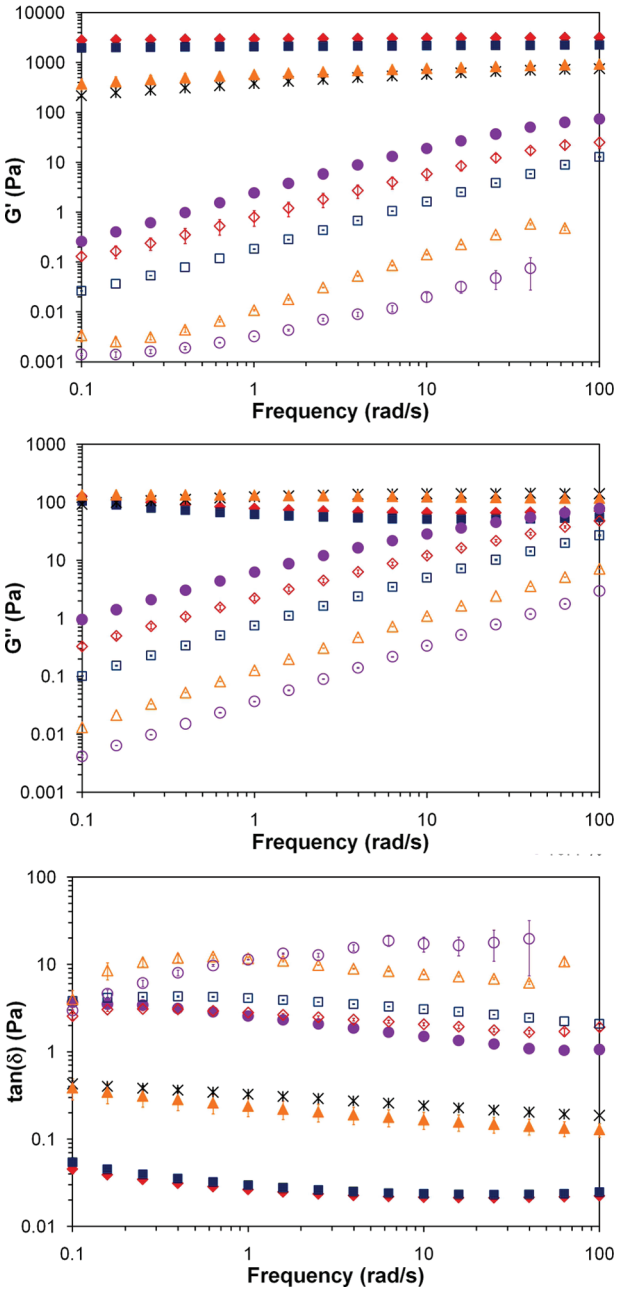


**Figure 8.** Linear viscoelastic properties of CNC suspensions at 17.3 vol % (red solid diamonds), 14.5 vol % (blue solid squares), 12.6 vol % (black stars), 12.1 vol % (orange solid triangles), 10.4 vol % (purple solid circles), 9.03 vol % (red open diamonds), 7.69 vol % (blue open squares), 6.30 vol % (orange open triangles), and 5.00 vol % (purple open circles).

**Viscoelastic Properties.** The storage modulus $G'$, loss modulus $G''$, and tangent of the phase angle $\tan \delta = G''/G'$ are shown in Figure 8. The samples with concentrations of 10.4 vol % and lower behaved as predominantly viscous fluids ($\tan \delta > 1$); coincidently, this was the highest concentration that appeared biphasic under cross-polarized optical microscopy. For the 12.1 and 12.6 vol % samples, an elastic behavior was dominant ($\tan \delta < 1$), but there was some dependence of $G'$ on $\omega$. The frequency independence of $G'$ did occur at 14.5 and 17.3 vol % CNCs, indicating a stiff gel behavior. Thus, at the temperature

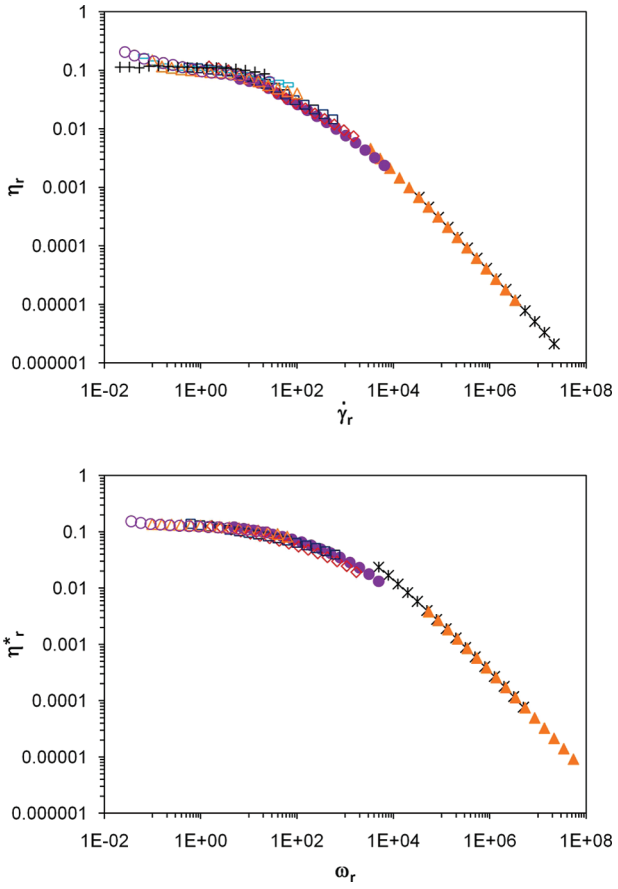


**Figure 9.** Time−concentration superposition of the viscosities of CNC suspensions at 12.6 vol % (black stars), 12.1 vol % (orange solid triangles), 10.4 vol % (purple solid circles), 9.03 vol % (red open diamonds), 7.69 vol % (blue open squares), 6.99 vol % (aqua open rectangles) 6.30 vol % (orange open triangles), 5.00 vol % (purple open circles), and 3.07 vol % (black crosses).

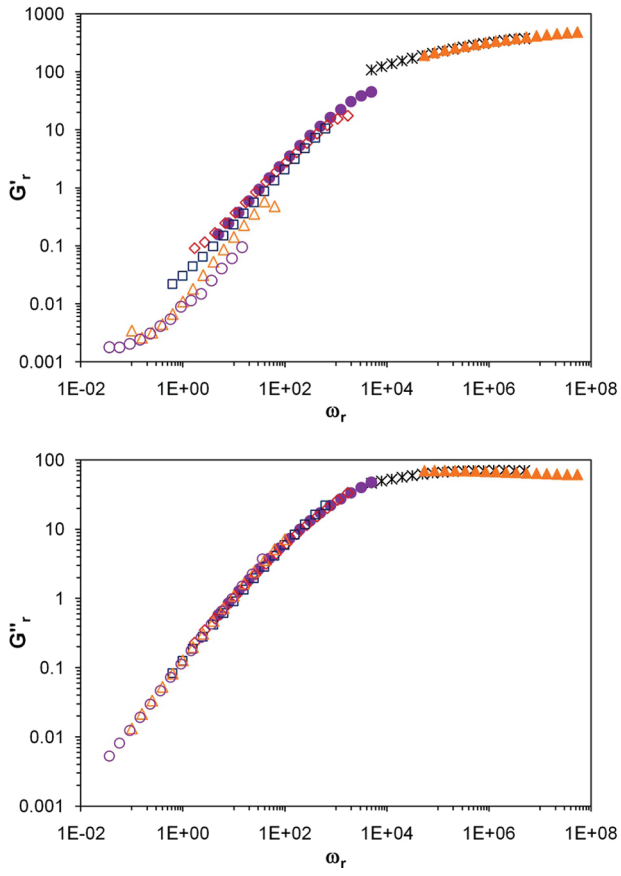


**Figure 10.** Time−concentration superposition of the viscoelastic properties of CNC suspensions at 12.6 vol % (black stars), 12.1 vol % (orange solid triangles), 10.4 vol % (purple solid circles), 9.03 vol % (red open diamonds), 7.69 vol % (blue open squares), 6.30 vol % (orange open triangles), and 5.00 vol % (purple open circles).

used for the rheological measurements (10 °C), the transition to a gel occurred between 12.6 and 14.5 vol %. These results support the hypothesis that the loss of fingerprint texture between 12.1 and 14.5 vol % (Figure 4), and change in power law behavior (Table 1) between 12.6 and 14.5 vol % were due to a liquid crystal to gel transition.

To determine if the gels were an equilibrium structure, a long amplitude oscillatory shear (LAOS) experiment was performed on the 14.5 vol % sample at 20% strain to disturb the structure of the suspension. The $G'$ measured during LAOS was 50% smaller than the one obtained with a 1.5% strain (in the LVE). After resting for 40 min the $G'$, measured within the LVE, was only 5% lower than original, and after 80 min the recovery was complete within experimental error. This result indicates that the gels are equilibrium structures (data shown in Figure S7 of the Supporting Information).

**Data Reduction.** Figure 9 shows that below the liquid crystalline to gel transition both the steady shear and complex viscosity data could generally be reduced to a master curve. The master curves were prepared by plotting the reduced viscosities, defined as $\eta^*_r = (\eta^* b_c)/a^*_c$ and $\eta_r = (\eta b_c)/a_c$, versus the reduced frequency $\omega = \omega a^*_c$ and reduced shear rate $\dot{\gamma}_r = \dot{\gamma} a_c$, where $\eta$ is the steady shear viscosity, $\eta^*$ is the complex viscosity, $\dot{\gamma}$ is the shear rate, $\omega$ is the frequency, $b_c = c_{ref}/c$ is a stress shift factor, and $a^*_c = (\eta^*_0/\eta^*_{0,ref})(c_{ref}/c)$ and $a_c = (\eta_0/\eta_{0,ref})(c_{ref}/c)$ are inverse time shift factors; $c$ is the CNC concentration. For the subscripts, 0 refers to the Newtonian plateau value, r to a reduced variable, and ref the reference concentration, which was chosen to be 6.30 vol %. There was a slight deviation in reduced steady shear viscosity at low shear rate for the predominantly isotropic 3.07 vol % suspension. For the complex viscosity, the data collapsed on a master curve up to a concentration of 10.4 vol %, but a discontinuity occurred afterward. This was also the highest concentration at which an isotropic section was detected using cross-polarized microscopy; therefore, the discontinuity may be related to a change in the relaxation mechanism caused by a phase transition.

Time−concentration superpositions of $G'$ and $G''$ were also attempted by plotting the reduced storage $G'_r = G'b_c$ and loss $G''_r = G''b_c$, moduli against the reduced frequency. The superposition results are shown in Figure 10. For most of the frequency range, $G'$ did not collapse onto a master curve; however, $G''$ did collapse satisfactorily. An analogous behavior was observed by Lee and Brant in biphasic xanthan solutions.[36] For their samples, $G''$ and $\eta^*$ collapsed onto a master curve, but $G'$ and $\eta$ did not; they suggested that the relaxation mechanism varied with concentration under steady shear conditions, but under oscillatory shear the relaxation processes were the same regardless of the microstructure. However, these authors did not provide an

explanation for why the storage modulus did not conform to a master curve. The data suggest that the elastic relaxation of CNC suspensions was modified as the morphology and total interfacial area between liquid crystalline and isotropic regions vary but that the viscous relaxation was unaffected by these microstructural changes.

As previously mentioned, cross-polarized optical microscopy showed that with increasing concentration the microstructure of the suspensions changed from dispersed liquid crystalline domains in a continuous isotropic matrix, to a seemingly cocontinuous blend, then to dispersed droplets of isotropic domains in a continuous liquid crystalline phase, followed by a totally liquid crystalline material and finally to a gel. This microstructural evolution impacts the relaxation times and mechanisms but has a smaller effect on $G''$ than $G'$. This behavior is analogous to that observed in mixtures of immiscible phases where the interfacial tension contributes to the viscoelastic properties.[37] The relaxation of a droplet after it is deformed affects mostly the elastic component, while the viscous contribution is very small.[38] The effect is larger as the interfacial tension and area increase; the latter clearly varies depending on the volume of the anisotropic phase.[39] Although the $G'$ data did not collapse uniformly, the general shape of the $G'_r$ versus $\omega_r$ curve resembled what would be expected for a blend of two immiscible Maxwell fluids. This model is simplistic for the complexity of the system, but it is useful to visualize the effects of interfacial tension. There is evidence of a plateau or shoulder at low values of $\omega_r$ and a second plateau at high $\omega_r$; the low-frequency plateau is attributed to the elastic contribution of the interface.[39] At intermediate frequencies the highest slope is 1.15, which deviates from the expected value of 2.[39] In the case of $G''$, the slope at low frequencies is 0.97, which approximates the expected value of 1 for an immiscible blend of two Maxwell fluids.[39]

**Viscosity and Moduli versus Concentration.** One of the hallmarks of polymeric lyotropic suspensions is that the low shear viscosity versus concentration goes through a maximum in the biphasic region, and the magnitude of this maximum decreases with increasing shear rate.[31,40] This maximum is presumed to occur because when the sample is predominantly isotropic the resistance to flow increases with increasing concentration. However, at some concentration in the biphasic region, the increasing order resulting from the increasing fraction of liquid crystalline domains causes the viscosity to decrease with concentration. Similar behavior has also been reported for the elastic and viscous moduli.[31,40]

Figure 11a shows the steady shear and complex viscosities as a function of concentration; the phase boundaries are based on microscopic observation. Surprisingly, no maxima are observed in the biphasic region, although a change in the slope is detected at 7.69 vol %. Instead, both $\eta^*$ and $G'$ show slight local maxima at 12.1 vol %; based on optical microscopy, this concentration is purely liquid crystalline. Increasing the concentration into the gel region results in a plateau for both $\eta^*$ and $G'$. No maximum was observed for the steady shear viscosity; this may suggest that the ordering is so tenuous as to be disrupted by a shear rate of 0.1 $s^{-1}$. While the origin of this unexpected behavior is not evident, it is interesting that another CNC system also deviated from the typical behavior. Bercea and Navard reported that micrometer length CNC showed only a very small reduction in viscosity at the critical concentration where the sample became biphasic followed by a monotonic increase with concentration.[18] It is possible that changes in attractive interactions caused by variations in the ionic strength with increasing CNC concentration result in this anomalous behavior. This will be explored in future research.

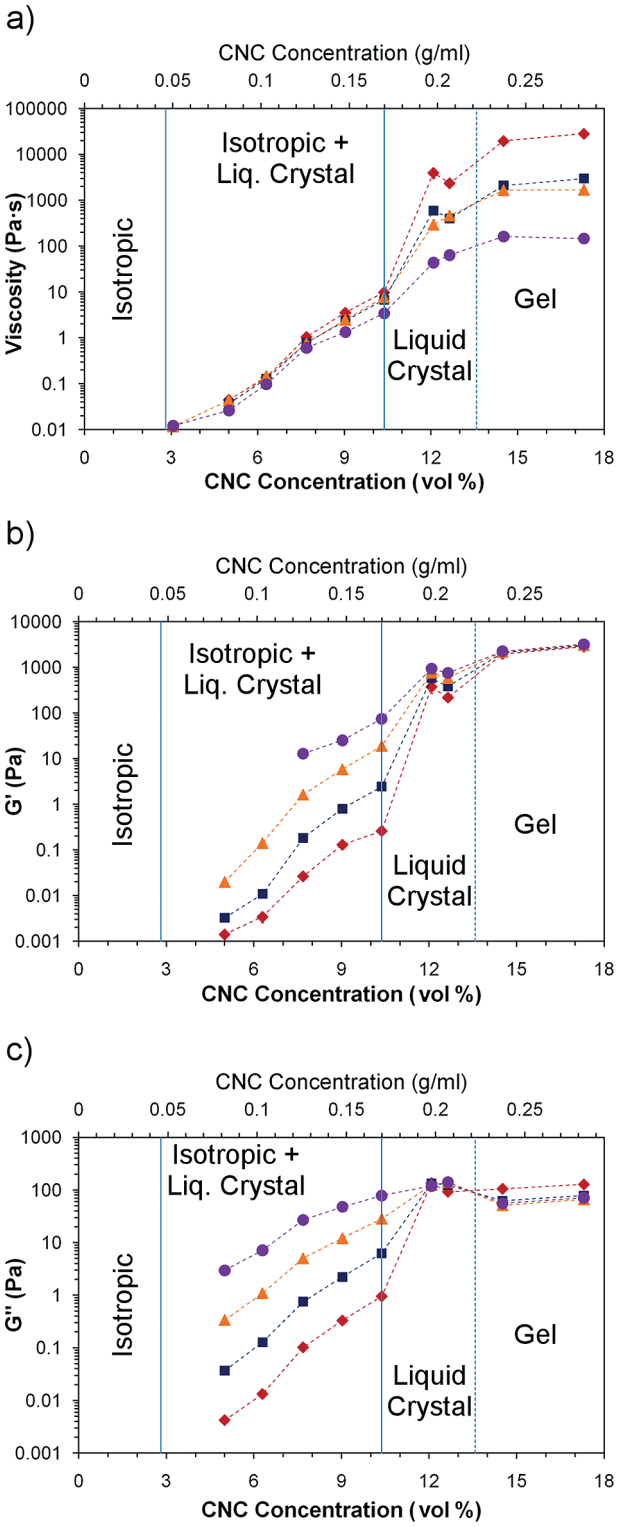


**Figure 11.** Rheological properties versus concentration. (a) Complex and steady shear viscosities at 0.1 rad/s (red diamonds), 1.0 rad/s (blue squares), 0.1 $s^{-1}$ (orange triangles), and 1 $s^{-1}$ (purple circles); (b) storage modulus; and (c) loss modulus at 0.1 rad/s (red diamonds), 1.0 rad/s (blue squares), 10 rad/s (orange triangles), and 100 rad/s (purple circles). The solid vertical lines indicate a phase transition; the discontinuous vertical line indicates that the liquid crystal to gel transition is approximate.


dx.doi.org/10.1021/ma201649f |*Macromolecules* 2011, 44, 8990–8998

## CONCLUSIONS

Aqueous dispersions of sulfonated CNC produced from cotton show lyotropic phase behavior. Based on cross-polarized optical microscopy using a 20× objective, 10.4 vol % < $\phi_{LC}$ < 12.1 vol %. A $\phi_{LC}$ measurement could not be obtained through macroscopic imaging because of the poor separation between isotropic and liquid crystalline domains in the biphasic region; nevertheless, it was possible to measure the volume fraction of anisotropic phase up to a value 0.6. Liquid crystalline samples exhibited the fingerprint texture characteristic of a cholesteric liquid crystal. Between 12.6 and 14.5 vol % the system transitioned to a birefringent gel. Temperature had a marked influence on phase behavior between 35 and 40 °C but not at lower temperatures. A time−concentration superposition could be obtained for $G''$ but not for $G'$; this suggests a change of the elastic relaxation mechanism within the biphasic region as the morphology and interfacial area are varied. This behavior is analogous to mixtures of immiscible polymer melts where the contribution of the interface to $G''$ and $\eta^*$ is small. Consistent with expectations for lyotropic polymer solutions, biphasic and liquid crystalline samples showed three-region rheological behavior and a failure of the Cox−Merz rule. However, plots of viscosity and moduli versus concentration did not show the expected maxima in the biphasic region. These results highlight that while nanorod dispersions have many parallels with rodlike polymer solutions the complications of electrostatic interactions and polydispersity can result in unusual behaviors.

## ASSOCIATED CONTENT

**Supporting Information.** Additional cross-polarized microscopy images of various CNC suspensions rotated 0°, 45°, and 90°; cross-polarized microscopy pictures at 24, 35, and 40 °C of a 12.1 vol % CNC suspension; theoretical calculations based on the SLO theory and gel reset experiments. This material is available free of charge via the Internet at http://pubs.acs.org.

## AUTHOR INFORMATION

**Corresponding Author**
*Phone (864) 656-2131. E-mail ckitche@clemson.edu.

## ACKNOWLEDGMENT

C.L.K. acknowledges the Center for Advanced Engineering Fibers and Films at Clemson University for support and the Graduate School at Clemson University for PSA-NGGF fellowship. V.A.D. acknowledges National Science Foundation CAREER CMMI-0846629 and Fluid Dynamics Grants CBET-0854010.

## REFERENCES

(1) Eichhorn, S. J.; Dufresne, A.; Aranguren, M.; Marcovich, N. E.; Capadona, J. R.; Rowan, S. J.; Weder, C.; Thielemans, W.; Roman, M.; Renneckar, S.; Gindl, W.; Veigel, S.; Keckes, J.; Yano, H.; Abe, K.; Nogi, M.; Nakagaito, A. N.; Mangalam, A.; Simonsen, J.; Benight, A. S.; Bismarck, A.; Berglund, L. A.; Peijs, T. *J. Mater. Sci.* **2010**, *45*, 1–33.
(2) Azizi Samir, M. A. S.; Alloin, F.; Dufresne, A. *Biomacromolecules* **2005**, *6*, 612–626.
(3) Shopsowitz, K. E.; Qi, H.; Hamad, W. Y.; MacLachlan, M. J. *Nature* **2010**, *468*, 422–425.
(4) Cranston, E. D.; Gray, D. G. *Biomacromolecules* **2006**, *7*, 2522–2530.
(5) Beck-Candanedo, S.; Roman, M.; Gray, D. G. *Biomacromolecules* **2005**, *6*, 1048–1054.
(6) Revol, J.-F.; Godbout, L.; Dong, X.-M.; Gray, D. G.; Chanzy, H.; Maret, G. *Liq. Cryst.* **1994**, *16*, 127–134.
(7) Liu, D.; Chen, X.; Yue, Y.; Chen, M.; Wu, Q. *Carbohydr. Polym.* **2011**, *84*, 316–322.
(8) Habibi, Y.; Lucia, L. A.; Rojas, O. J. *Chem. Rev.* **2010**, *110*, 3479–3500.
(9) De Souza Lima, M. M.; Borsali, R. *Macromol. Rapid Commun.* **2004**, *25*, 771–787.
(10) Ureña-Benavides, E. E.; Brown, P. J.; Kitchens, C. L. *Langmuir* **2010**, *26*, 14263–14270.
(11) Pan, J.; Hamad, W.; Straus, S. K. *Macromolecules* **2010**, *43*, 3851–3858.
(12) Ureña-Benavides, E. E.; Kitchens, C. L. *Macromolecules* **2011**, *44*, 3478–3484.
(13) Dong, X. M.; Revol, J.; Gray, D. G. *Cellulose* **1998**, *5*, 19–32.
(14) Hirai, A.; Inui, O.; Horii, F.; Tsuji, M. *Langmuir* **2009**, *25*, 497–502.
(15) Dong, X. M.; Kimura, T.; Revol, J.; Gray, D. G. *Langmuir* **1996**, *12*, 2076–2082.
(16) Dong, X. M.; Gray, D. G. *Langmuir* **1997**, *13*, 2404–2409.
(17) Orts, W. J.; Godbout, L.; Marchessault, R. H.; Revol, J.-F. *Macromolecules* **1998**, *31*, 5717–5725.
(18) Bercea, M.; Navard, P. *Macromolecules* **2000**, *33*, 6011–6016.
(19) Kvien, I.; Tanem, B. S.; Oksman, K. *Biomacromolecules* **2005**, *6*, 3160–3165.
(20) Villarrubia, J. S. *J. Res. Natl. Inst. Stand. Technol.* **1997**, *102*, 425–454.
(21) Terech, P.; Chazeau, L.; Cavaillé, J. Y. *Macromolecules* **1999**, *32*, 1872–1875.
(22) Elazzouzi-Hafraoui, S.; Nishiyama, Y.; Putaux, J.; Heux, L.; Dubreuil, F.; Rochas, C. *Biomacromolecules* **2008**, *9*, 57–65.
(23) Davis, V. A. *J. Mater. Res.* **2011**, *26*, 140.
(24) Odijk, T. *Macromolecules* **1986**, *19*, 2313–2329.
(25) Stroobants, A.; Lekkerkerker, H. N. W.; Odijk, T. *Macromolecules* **1986**, *19*, 2232–2238.
(26) Ao, G.; Nepal, D.; Aono, M.; Davis, V. A. *ACS Nano* **2011**, *5*, 1450–1458.
(27) Onogi, S.; Asada, T. In *Rheology and Rheo-optics of Polymer Liquid Crystals*; Astarita, G., Marrucci, G. Nicolais, L., Eds.; Proceedings of the Eighth International Congress on Rheology; Plenum Press: Napoles, Italy, 1980; pp 126−136.
(28) Burghardt, W. R. *Macromol. Chem. Phys.* **1998**, *199*, 471–488.
(29) Hongladarom, K.; Burghardt, W. R. *Rheol. Acta* **1998**, *37*, 46–53.
(30) Walker, L. *J. Rheol.* **1994**, *38*, 1525–1547.
(31) Larson, R. G. *The Structure and Rheology of Complex Fluids*; Oxford University Press: New York, 1999.
(32) Montesi, A.; Peña, A.; Pasquali, M. *Phys. Rev. Lett.* **2004**, *92*, 058303−1–058303−4.
(33) Davis, V. A.; Ericson, L. M.; Parra-Vasquez, A.; Fan, H.; Wang, Y.; Prieto, V.; Longoria, J. A.; Ramesh, S.; Saini, R. K.; Kittrell, C.; Billups, W. E.; Adams, W. W.; Hauge, R. H.; Smalley, R. E.; Pasquali, M. *Macromolecules* **2004**, *37*, 154–160.
(34) Doi, M.; Edwards, S. F. In *The Theory of Polymer Dynamics*; Oxford University Press: New York, 1986; pp 289−380.
(35) Papkov, S. P.; Kulichikhin, V. G.; Kalmykova, V. D.; Malkin, A. Y. *J. Polym. Sci., Polym. Phys. Ed.* **1974**, *12*, 1753–1770.
(36) Lee, H.; Brant, D. A. *Macromolecules* **2002**, *35*, 2212–2222.
(37) Vinckier, I.; Laun, H. M. *J. Rheol.* **2001**, *45*, 1373–1385.
(38) Tucker, C. L., III; Moldenaers, P. *Annu. Rev. Fluid Mech.* **2002**, *34*, 177–210.
(39) Graebling, D.; Muller, R.; Palierne, J. F. *Macromolecules* **1993**, *26*, 320–329.
(40) Marrucci, G. In *Liquid Crystallinity in Polymers*, Ciferri, A., Ed.; VCH Publishers: New York, 1991; pp 395−421.